REPORT DOCUMENTATION PAGE

Form Approved
OMB NO. 0704-0188

Public reporting burden for this collection of information is estimated to average 1 hour per response, including the time for reviewing instructions, searching existing data sources, gathering and maintaining the data needed, and completing and reviewing the collection of information. Send comment regarding this burden estimates or any other aspect of this collection of information, including suggestions for reducing this burden, to Washington Headquarters Services, Directorate for information Operations and Reports, 1215 Jefferson Davis Highway, Suite 1204, Arlington, VA 22202-4302, and to the Office of Management and Budget, Paperwork Reduction Project (0704-0188), Washington, DC 20503.

1. AGENCY USE ONLY (Leave blank)	2. REPORT DATE 8/21/00	3. REPORT TYPE AND DATES COVERED April 1, 1998 - Final Technical Report March 31, 2000

4. TITLE AND SUBTITLE

Semiconductor In-line Fiber Devices for Optical Communication Systems

5. FUNDING NUMBERS

N00014-98-1-0537

6. AUTHOR(S)

J. S. Harris, Principal Investigator

7. PERFORMING ORGANIZATION NAMES(S) AND ADDRESS(ES)

Stanford University

8. PERFORMING ORGANIZATION REPORT NUMBER

9. SPONSORING / MONITORING AGENCY NAME(S) AND ADDRESS(ES)

U.S. Army Research Office
P.O. Box 12211
Research Triangle Park, NC 27709-2211

10. SPONSORING / MONITORING AGENCY REPORT NUMBER

11. SUPPLEMENTARY NOTES

The views, opinions and/or findings contained in this report are those of the author(s) and should not be construed as an official Department of the Army position, policy or decision, unless so designated by other documentation.

12a. DISTRIBUTION / AVAILABILITY STATEMENT

Approved for public release; distribution unlimited.

12 b. DISTRIBUTION CODE

13. ABSTRACT *(Maximum 200 words)*

See attached

14. SUBJECT TERMS

15. NUMBER IF PAGES

30

16. PRICE CODE

17. SECURITY CLASSIFICATION OR REPORT	18. SECURITY CLASSIFICATION OF THIS PAGE	19. SECURITY CLASSIFICATION OF ABSTRACT	20. LIMITATION OF ABSTRACT
UNCLASSIFIED	UNCLASSIFIED	UNCLASSIFIED	UL

Semiconductor In-line Fiber Devices for Optical Communication Systems

Final Technical Report

J. S. Harris
Principal Investigator

For the period:

April 1, 1998 - March 31, 2000

Stanford University

Stanford, CA

1

20000829 166

DTIC QUALITY INSPECTED 4

Chapter 1 Introduction

A high-performance optical communication system requires high-performance optoelectronic devices. The conventional approach to fabricating fiber-coupled devices involves the interruption of the fiber and the insertion of the device. Several drawbacks are associated with this approach, including high insertion loss, mechanical instability, and high packaging costs. In-line fiber devices, in which light is evanescently coupled between single mode fibers and multimode high index waveguides, offer solutions to these problems. Materials that have been used in the implementation of in-line fiber devices include liquid crystals, electro-optic polymers and lithium niobate substrates. Gallium arsenide and other compound semiconductor devices offer significant advantages over the above materials in that they can be monolithically integrated with lasers and high-speed electronics, thereby reducing fabrication costs. In addition, the sharp index contrast between the semiconductor and the fiber leads to wavelength-selective coupling, which can be exploited for WDM applications.

The goal of this project is to demonstrate various compound semiconductor in-line fiber devices. The operation of these devices requires evanescent wave coupling, and hence phase-matching, between a side-polished single mode fiber and a high-index semiconductor waveguide. The large index contrast between the semiconductor and the fiber can be overcome by the use of dielectric mirrors in the semiconductor waveguide. The mirrors can be designed to provide high reflection for a specific mode angle, therefore the optical wave inside the semiconductor waveguide can propagate with an effective index much lower than the material index. This class of optical waveguides, where guiding is achieved by reflections from dielectric mirrors rather than total internal reflection at dielectric interfaces, is commonly referred to as anti-resonant reflecting optical waveguides (ARROW). By incorporating quantum well absorption/gain layers in the core of the ARROW, active devices such as modulators, detectors and light emitters can be realized in this configuration. This generic diagram of the devices described in this report is shown in Figure 1-1.
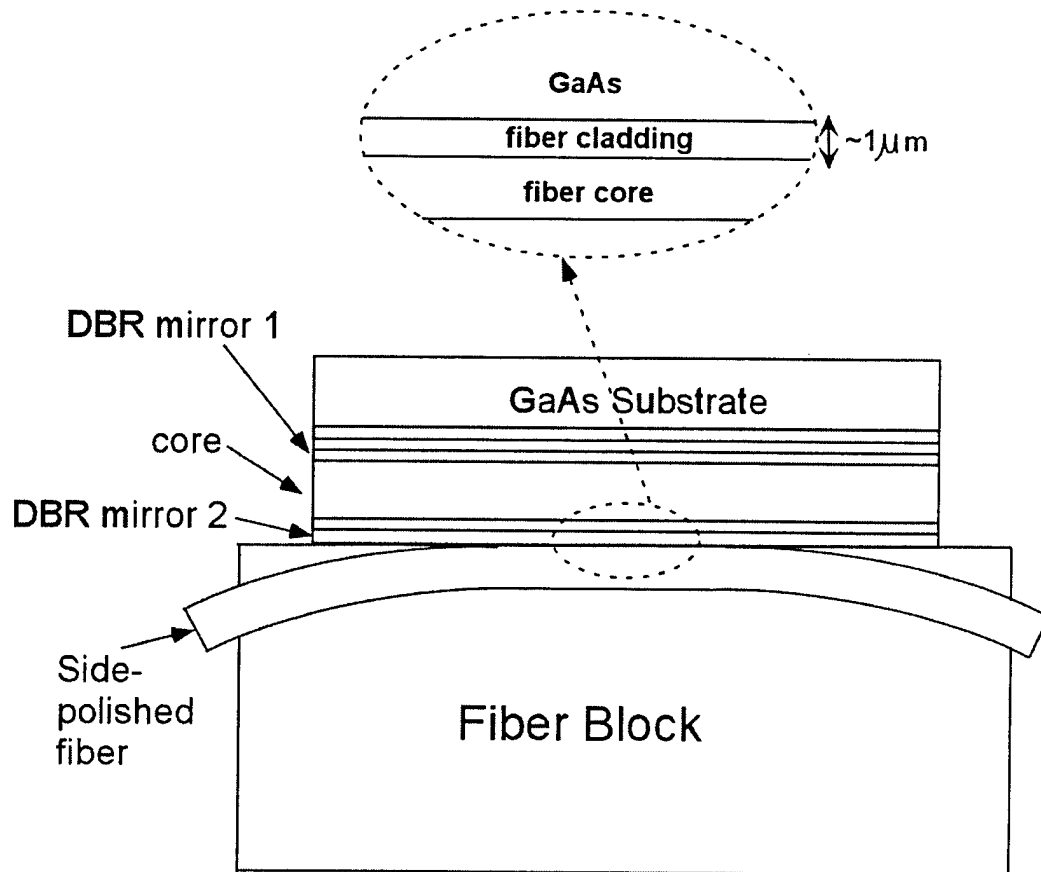
Figure 1-1. The schematic of a GaAs in-line fiber device. The fiber is side-polished so that the remaining cladding thickness is about 1μm.

The organization of this report is as follows. Chapter 2 focuses on passive wavelength selective devices, including narrow linewidth filters and detectors. Chapter 3 highlights the design and demonstration of multiple-quantum-well modulators based on the quantum confined Stark effect. The results from a light-emitting device are shown in Chapter 4. Finally, chapter 5 provides a brief summary of this work.

Chapter 2 In-line fiber filter and detector

2.1 In-line fiber filter

Wavelength division multiplexing (WDM) increases the channel capacity of a fiber-optic system by transmitting multiple wavelengths over a single fiber. It is therefore desirable to have a simple method of extracting a specific wavelength without disturbing others going through the fiber. This is especially useful for such systems as multiprocessor interconnects for parallel-processing computers and local area networks (LAN's) with ring topologies.

One way to achieve this goal is to use an asymmetric waveguide coupler consisting of a single-mode fiber and a semiconductor ARROW. At certain discrete wavelengths, light is coupled from the fiber into the ARROW, due to phase-matching conditions. The large difference in the dispersion characteristics between the guides results in very sharp resonances at phase-matched wavelengths. In addition, the in-line architecture is a highly efficient fiber interface, with low insertion loss and good mechanical stability.
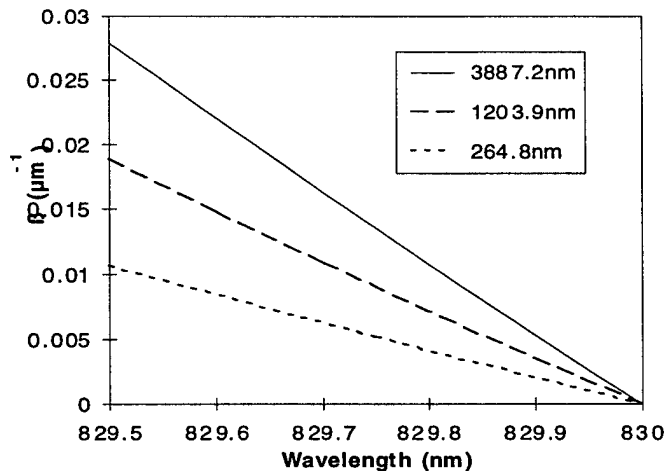
2.1.1 Device design

Fig. 2-1. The calculated difference in propagation constants between the fiber mode and the TE ARROW mode. The three curves represent three ARROWs with the same DBR (as the one shown in Fig. 2-2) but different core thicknesses (core material = $Al_{0.33}Ga_{0.67}As$). The unit for y-axis is μm^{-1}.

4

The resonance linewidth of an ARROW-fiber coupler is a function of the dispersion properties and the propagation loss of the ARROW, as well as the coupling strength between the waveguides. The dispersion of an ARROW is determined solely by its layer structure and can be controlled more easily than the other factors under our experimental arrangements, which will be described in the next section. As shown in Fig. 2-1, the propagation constant of an ARROW becomes more sensitive to wavelength changes as the core thickness increases.
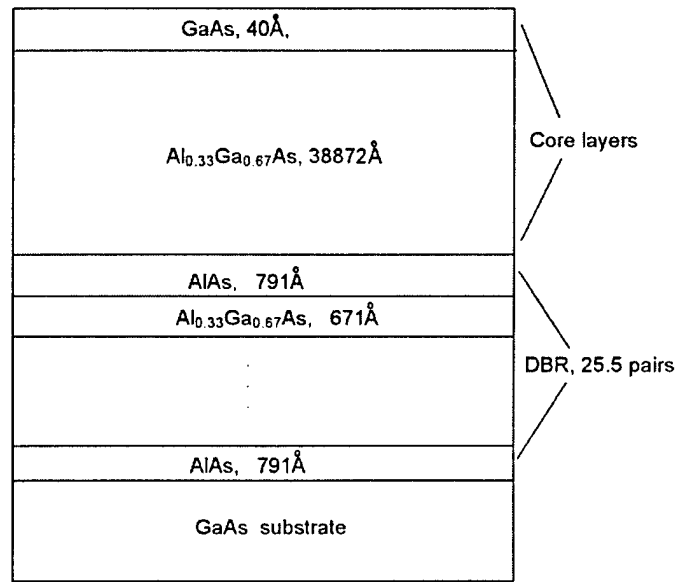

Fig. 2-2. The epitaxial structure of the ARROW used in the filter.

The epitaxial structure of the ARROW is shown in Fig. 2-2. All layers are undoped. An $Al_{0.33}Ga_{0.67}As$ core of $3.887\mu m$ was chosen for this experiment. $Al_{0.33}Ga_{0.67}As$ was used because its absorption onset wavelength is well below the operating wavelength of 830nm. The core thickness was chosen to minimize the linewidth, while keeping the MBE growth time within a reasonable limit. The $AlAs/Al_{0.33}Ga_{0.67}As$ DBR was designed to provide maximum reflectance at an incident angle of 25 degrees, which is the mode angle needed for phase-matching to a single-mode fiber. The calculated dispersion curves for the ARROW are shown in Fig. 2-3, showing phase-matching conditions at 818nm (TM) and 830nm (TE).
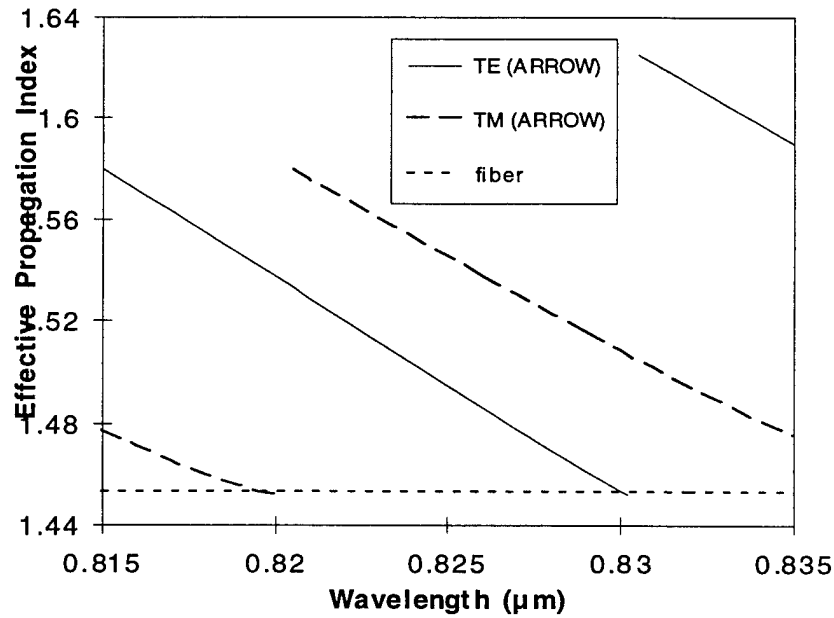
5

Fig. 2-3. The calculated dispersion curves for the single mode fiber and the highest order confined modes of the ARROW. The y-axis shows the effective propagation indices.

2.1.2 Experiment

Following MBE growth, the ARROW wafer was cleaved into pieces for testing. During testing, a polished fiber half coupler (from Canadian Instrumentation and Research Ltd.) was mounted on an x-y-z stage and positioned on top of the ARROW piece. The fiber half coupler is made by epoxying a single mode fiber into a curved groove in a glass substrate and then polishing both the substrate and the fiber cladding to within a few microns of the fiber core. The polished interaction region is about 1mm in length. The ends of the fiber are spliced to patch cords, which can then be connected to other fibers, optical sources or testing instruments. The ARROW piece was placed on a thermoelectric temperature controller. Drops of index matching fluid (n=1.458), whose index was closely matched to that of the fiber cladding (n=1.452), were applied between the fiber block and the ARROW to ensure good optical contact. The optical source used was a fiber coupled GaAs (~830nm) laser diode biased just below threshold. A polarizer and a fiber polarization controller were used at the input end. The transmission spectra of the system were measured with a HP70951A optical spectrum analyzer. The experimental setup is shown in Fig. 2-4.
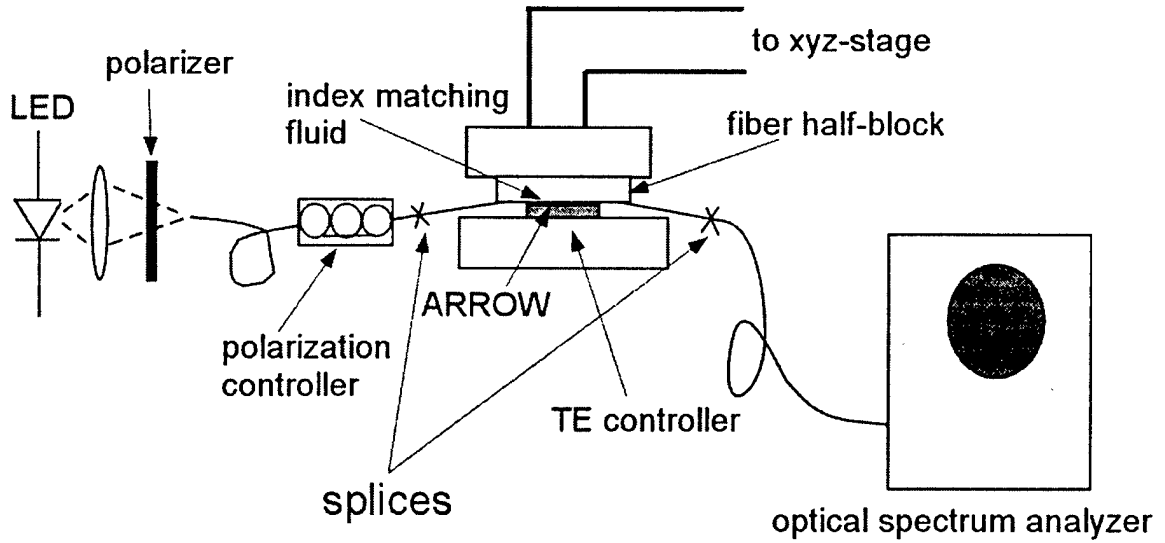
6

Fig. 2-4. The experimental setup for testing in-line fiber filters.

2.1.3 Results and discussion

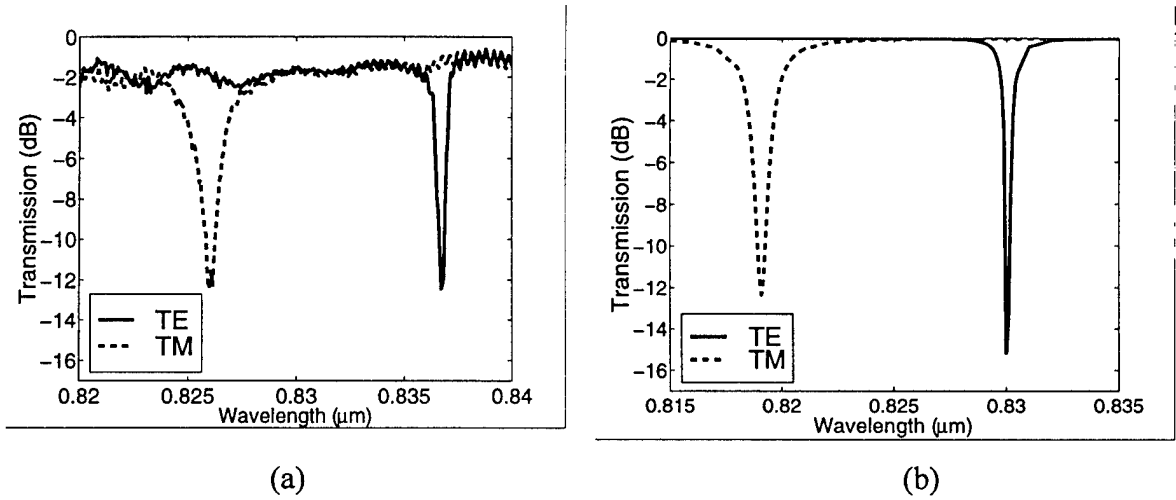(a)   (b)

Fig. 2-5. (a) The measured transmission spectra at 25°C; (b) The simulated spectra. The parameters used for the simulation are: $C = 0.005\mu m^{-1}$, $\alpha = 0.003\mu m^{-1}$ (TE), $\alpha = 0.018\mu m^{-1}$ (TM) .

Fig. 2-5a. shows the measured transmission spectra of the filter at 25°C. The TE dip has a full-width at half-maximum (FWHM) of 0.5nm and the TM dip has a FWHM of 1.3nm. The TM dip is broader because the DBR mirror reflectance is lower and hence the ARROW propagation loss is higher. Fig. 2-5b shows the simulated results. The

differences between the simulated and measured results are primarily due to the simplicity of the model (for example, the curvature of the interaction region is ignored). They can also be attributed to measurement errors (such as those due to the finite resolution bandwidth of the optical spectrum analyzer). The positions of the resonance dips are shifted from the design wavelengths due to thickness variations in MBE growth. The off-resonance insertion loss (~2dB) of the system is due to imperfect fiber splicing.

2.2 Wavelength selective in-line fiber photodetector

In some applications, once light at a specific wavelength is filtered out of a single-mode fiber, it is desirable to convert it into an electrical signal. This can be accomplished by incorporating absorbing quantum wells in the core of the ARROW, turning an in-line fiber filter into a photodetector. In addition to its wavelength-selective nature, this type of detector has a distributed absorbing structure which is conducive to high-speed, high-power operation. The in-line fiber interface also allows for low insertion loss and low cost packaging.

2.2.1 Device design

The epitaxial structure of the absorbing ARROW is shown in Fig. 2-6. Similar to conventional photodetectors, the DBR mirrors were doped to form a p-i-n structure, and an absorbing quantum well was placed in the intrinsic region. The doping concentrations are $1 \times 10^{19} cm^{-3}$ for the p-type layers and $1 \times 10^{18} cm^{-3}$ for the n-type layers. When the ARROW is attached to the polished fiber half coupler, optical waves can be guided in its core by reflection from the n-doped DBR mirror on the one side, and a combination of reflection from the p-doped DBR mirror and total internal reflection from the fiber cladding on the other side. The n-type and p-type DBR mirrors consist of 40 and 5 pairs of AlAs/Al$_{0.33}$Ga$_{0.67}$As quarter wave layers, respectively. The p-type mirror was designed to be partially reflective so that there is sufficient field overlap between the guided modes of the fiber and the ARROW. The core of the ARROW is made up of an Al$_{0.33}$Ga$_{0.67}$As layer and a 75Å GaAs quantum well. The quantum well was placed at the center of the core where the intensity peak of the guided ARROW mode occurs, in order to maximize the quantum efficiency.
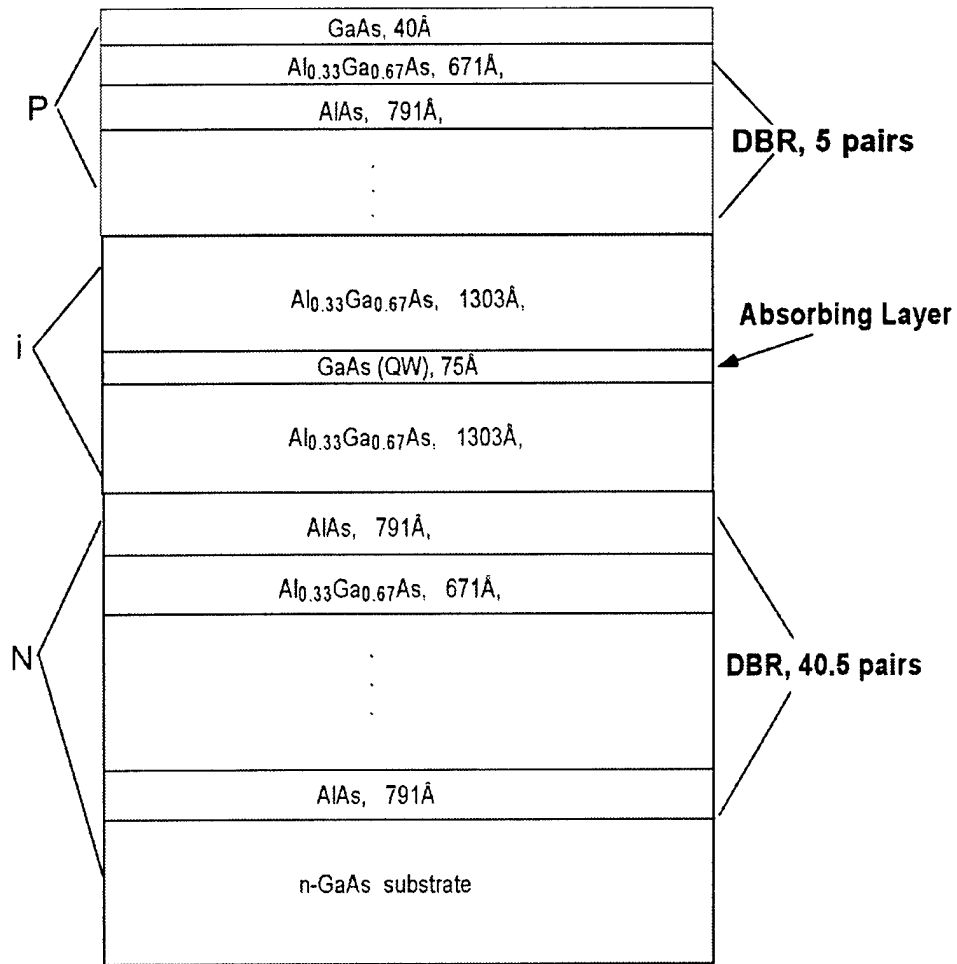
| GaAs, 40Å |
| Al$_{0.33}$Ga$_{0.67}$As, 671Å, |
| AlAs, 791Å, |
| . . . |

P — **DBR, 5 pairs**

| Al$_{0.33}$Ga$_{0.67}$As, 1303Å, |
| GaAs (QW), 75Å |
| Al$_{0.33}$Ga$_{0.67}$As, 1303Å, |

i — **Absorbing Layer**

| AlAs, 791Å, |
| Al$_{0.33}$Ga$_{0.67}$As, 671Å, |
| . . . |
| AlAs, 791Å |

N — **DBR, 40.5 pairs**

| n-GaAs substrate |

Fig. 2-6. The epitaxial structure of the ARROW used in the in-line detector.

2.2.2 Experiment

Individual devices were defined on the MBE-grown wafer by standard wet chemical etching (with a 1:5:160 mixture of H_2SO_4:H_2O_2:H_2O). Au/Ge/Ni/Au (400Å/125Å/120Å/1000Å) layers were evaporated on the backside of the substrate and thermally annealed (405°C for 30 seconds) to form a n-type ohmic contact. Patterned Ti/Au (250Å/1000Å) layers formed a p-type ohmic contact on top of each device. The wafer was then cleaved into pieces (4mm by 3mm). The setup that was used for filter testing (Fig. 2-4) was used here, with the addition of an infrared CCD camera which can be focused on the polished interaction region of the coupler. The position of the fiber core was determined by launching light from a tunable GaAs laser diode into the fiber half

coupler and observing the scattered light with the camera. After aligning the fiber core to the ARROW, the two waveguides were brought into contact, with index matching fluid applied at the interface. The tunable laser diode that was used for aligning then served as the light source for device testing. A 5V reverse bias was applied to the p-i-n junction within the ARROW and a 10kΩ series resistor. The photocurrent was obtained by measuring and converting the voltage that appeared across the resistor (Fig. 2-7).

(a)   (b)
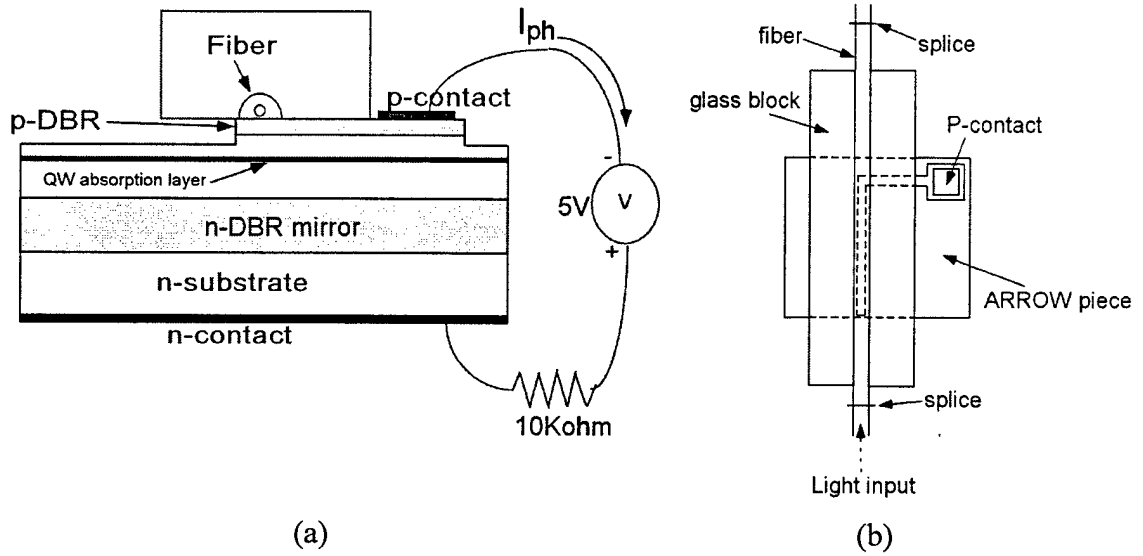
Fig. 2-7. Illustration of photodetector testing arrangement: (a) cross-sectional view, and (b) top view.

2.2.3 Results and discussion

Fig. 2-8a shows the photocurrent as a function of wavelength of TE-polarized light (electric field vector parallel to the plane of the GaAs substrate) traveling through the fiber. The response peaks at 816nm with a FWHM of 1.6nm. The laser power coupled into the input single mode fiber was about 42μW, which means our detector has an external quantum efficiency of 75%. The TE transmission spectrum of the device measured with an optical spectrum analyzer is shown in Fig. 2-8b. The broadband light source was the same laser diode biased below threshold. The resonance positions and shapes in the two figures are consistent with each other.

The off-resonance transmission of our device (Fig. 4-13b) is about 70%, with the loss coming from poor fiber splicing. By reversing the light traveling direction and

10

obtaining essentially the same photocurrent response, we concluded that each of the two splices had a power transmission of about 83% ($0.83^2 = 0.7$). Therefore, with a perfect splice, our detector would achieve an external quantum efficiency of more than 90%. The polarization sensitivity of the device could be eliminated by defining a ridge waveguide in the semiconductor (which compensates for the TE and TM modal dispersion) and using strained quantum wells (which equalizes the TE and TM absorption). By changing the quantum well material composition (from GaAs to InGaAs or GaInNAs), this device can operate at longer wavelengths and prove useful for low cost WDM applications.
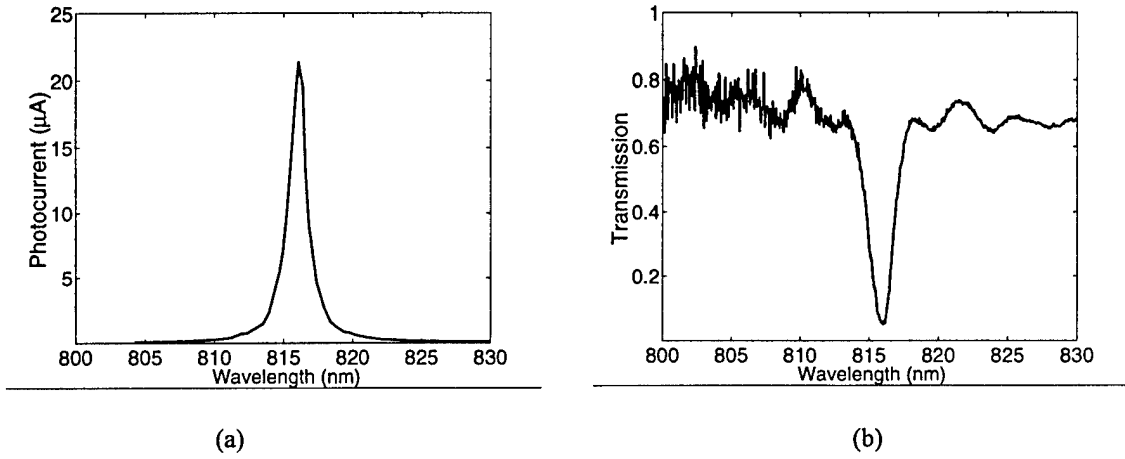

(a)   (b)

Fig. 2-8 (a) The measured photocurrent response. (b) The measured device transmission.

Chapter 3 In-line fiber modulator

3.1 Introduction

External optical modulators have an important role in high-speed photonic links because of their low chirp characteristics compared with directly modulated semiconductor lasers. In this chapter, the design and experimental demonstration of GaAs/AlGaAs optical intensity modulators based on the ARROW-fiber coupled waveguide structure are presented.

The shape and the position of the resonance dip in an ARROW-fiber system are functions of the refractive indices (both real and imaginary parts) of the ARROW layers. Therefore, by changing these refractive index values, the intensity of the light going through the fiber can be modulated.

The refractive index of a semiconductor structure can be modified through either bulk effects such as carrier injection, or quantum phenomena such as the quantum confined Stark effect (QCSE). As its name suggests, carrier injection requires the application of an injection current and is therefore less power efficient than the QCSE, which only requires the application of an electric field. As a result, the modulation mechanism chosen for our devices is the QCSE.

3.2 Device design

A simple way to realize in-line fiber light modulation is to use an ARROW which consists of a MQW core layer. By applying an electric field perpendicular to the plane of the quantum wells, the complex index of refraction of the MQW layer is changed through the QCSE, which results in both a shift in the phase-matched wavelength and a change in the shape of the resonance dip. Therefore, intensity modulation of the transmitted light through the fiber can be obtained.

GaAs, 40Å

$Al_{0.33}Ga_{0.67}As$, 696Å

AlAs, 818Å

⋮

P { DBR, 3 pairs

$Al_{0.33}Ga_{0.67}As$, 270Å

GaAs, 75Å

AlAs, 35Å

⋮

$Al_{0.33}Ga_{0.67}As$, 260Å

i { MQW, 32 pairs

AlAs, 818Å

$Al_{0.33}Ga_{0.67}As$, 696Å
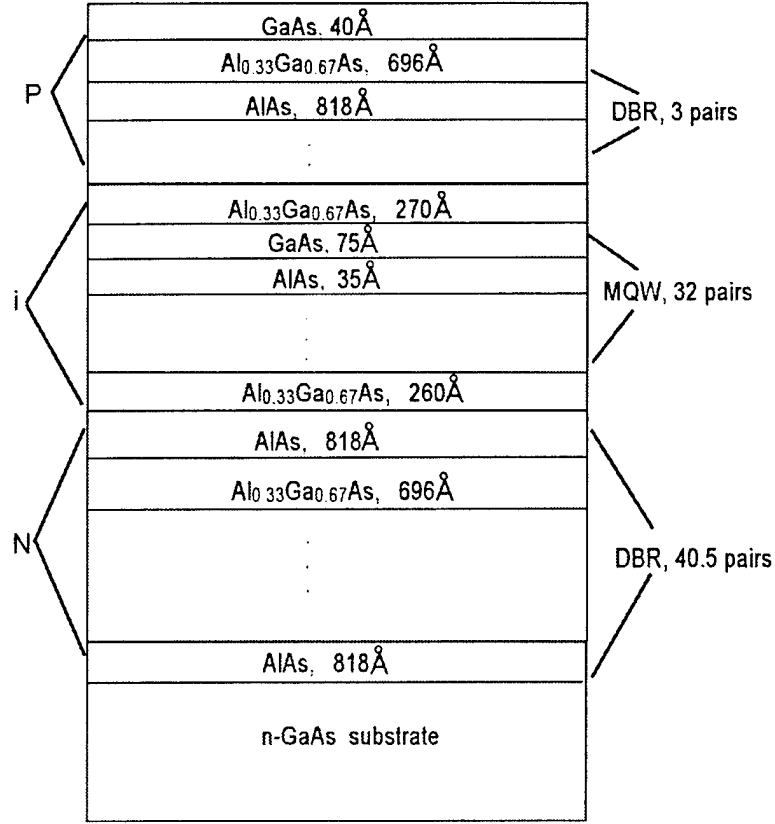
⋮

N { DBR, 40.5 pairs

AlAs, 818Å

n-GaAs substrate

Fig. 3-1. The detailed epitaxial structure of the double mirror ARROW structure. The intrinsic MQW core region is surrounded by a highly reflective DBR (n-doped) and a leaky DBR (p-doped).

The epitaxial structure of the ARROW is shown in Fig. 3-1. The doping concentrations are $1 \times 10^{19} cm^{-3}$ for the p-type layers and $1 \times 10^{18} cm^{-3}$ for the n-type layers. The experimentally determined field-dependent absorption coefficients and the calculated refractive indices for the quantum wells used in the ARROW are shown in Fig. 3-2 and Fig. 3-3 respectively. A 40kV/cm field corresponds to the built-in field of our diode structure. The designed phase-matched wavelength of the device is 855nm (for TE polarization), which is about 25nm longer than the first heavy-hole exciton resonance wavelength under zero bias. This is to ensure that the propagation loss in the ARROW is low enough for significant evanescent coupling to occur. The calculated effective indices for the ARROW and the fiber are shown in Fig. 3-4.
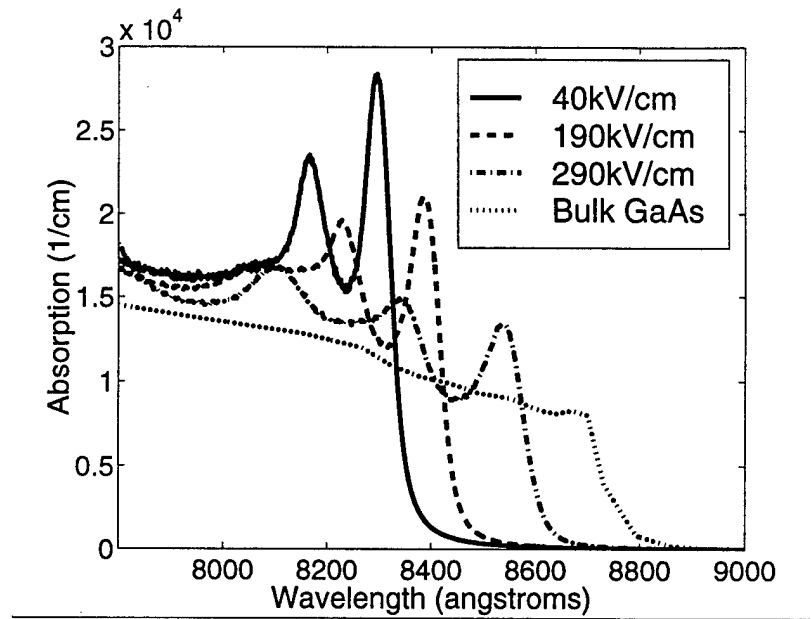
Fig. 3-2. The measured absorption spectra for 75Å GaAs quantum wells with 35Å AlAs barriers. The polarization of the light is TE (parallel to the MQW plane).
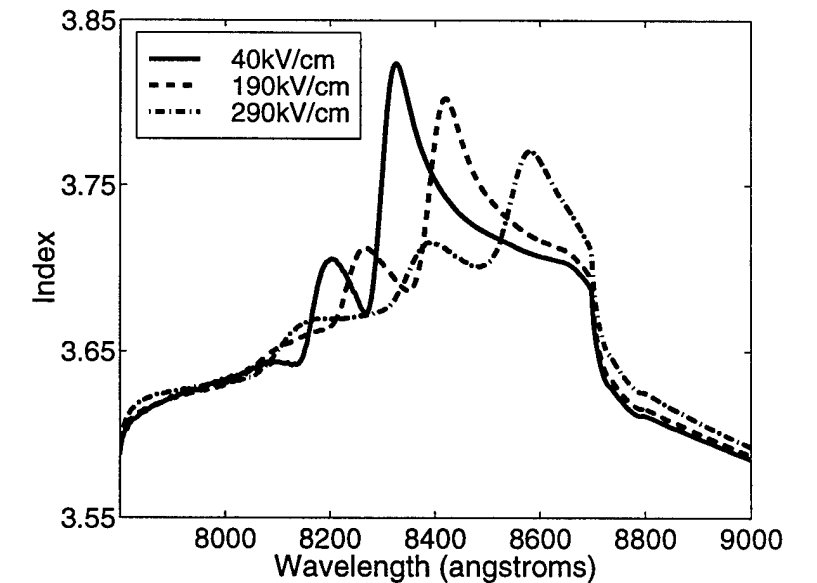

Fig. 3-3. The calculated refractive index for 75Å GaAs quantum wells with 35Å AlAs barriers. The index changes with respect to bulk GaAs values are calculated using the Kramers-Kronig relationship.
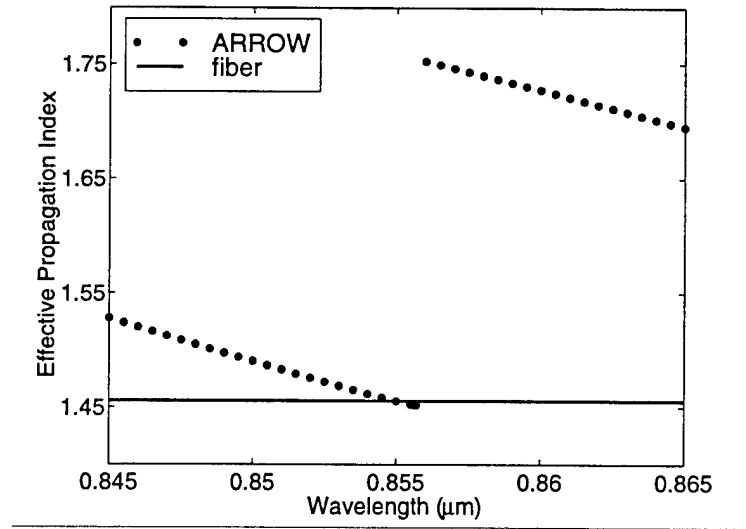
14

Fig. 3-4. The calculated TE effective propagation indices for the ARROW and the fiber. The ARROW mode is the highest order confined mode.

3.3 Experimental results

The TE transmission spectra of a typical device are shown in Fig. 3-5a. Due to thickness variations in MBE growth, the 0V phase-matched wavelength is 845.5nm instead of the designed 855nm. The off-resonance insertion loss of our device is about 3dB, which, as before, can be attributed to poor fiber splicing. As the applied bias is increased from zero, the real part of the MQW refractive index increases, resulting initially in a red-shift of the phase-matched wavelength. When the bias is large enough such that the first heavy-hole excitonic resonance coincides with the 0V phase-matched wavelength, the absorption in the MQW at that wavelength quenches the transmission dip. The maximum modulation contrast occurs at 845.5nm, where the device transmission changes from 10% to 40% with a 9V swing. As shown in Fig. 3-5b, the modulator has an essentially linear voltage-dependent transmission within certain voltage ranges (such as from 3 to 4.5V, or 6.5 to 7.5V), which lends itself for potential analog applications. The 4:1 on/off ratio at the 0V resonant wavelength also makes it attractive for digital or switching applications. In addition, compared with conventional electro-absorption modulators, this device is more suited for high-power applications because at

15

the high-absorption state of the MQW, most of the light stays in the fiber and very few carriers are generated in the ARROW.
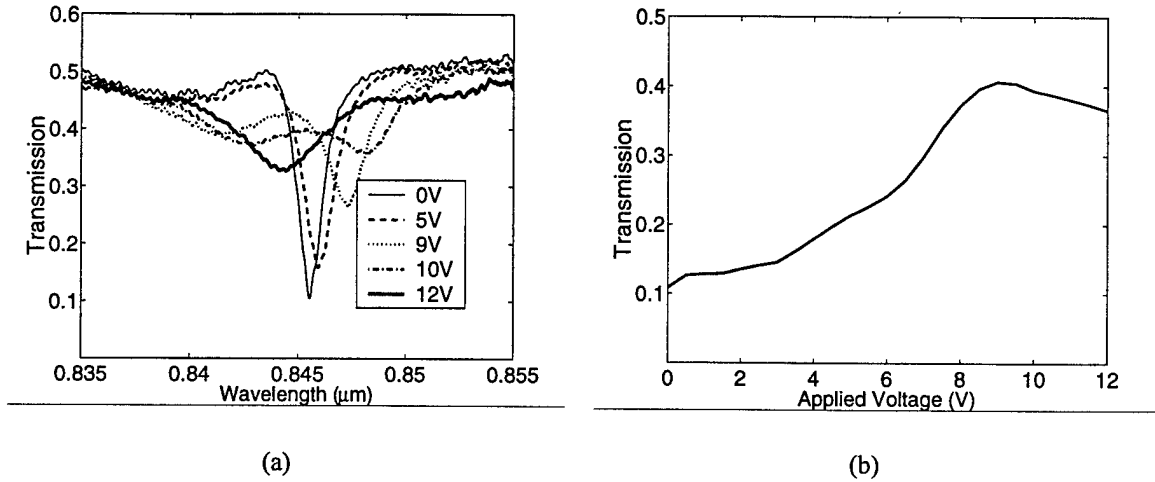

Fig. 3-5. (a) The transmission spectra of the modulator under different bias conditions. (b) Transmission at 845.5nm as a function of applied bias.

3.4 Discussion

The appearance of multiple dips in the transmission curves can be explained by the wavelength-dependent absorption coefficients of the MQW. When there is a variation in the MQW absorption (and thus, ARROW propagation loss) near the phase-matched wavelength, the shape of the transmission curve is no longer a simple dip. This behavior is illustrated in Fig. 3-6, where the transmission spectra are calculated by solving the coupled mode equations with assumed ARROW loss spectra, which are roughly based on the MQW absorption data shown in Fig. 3-2.
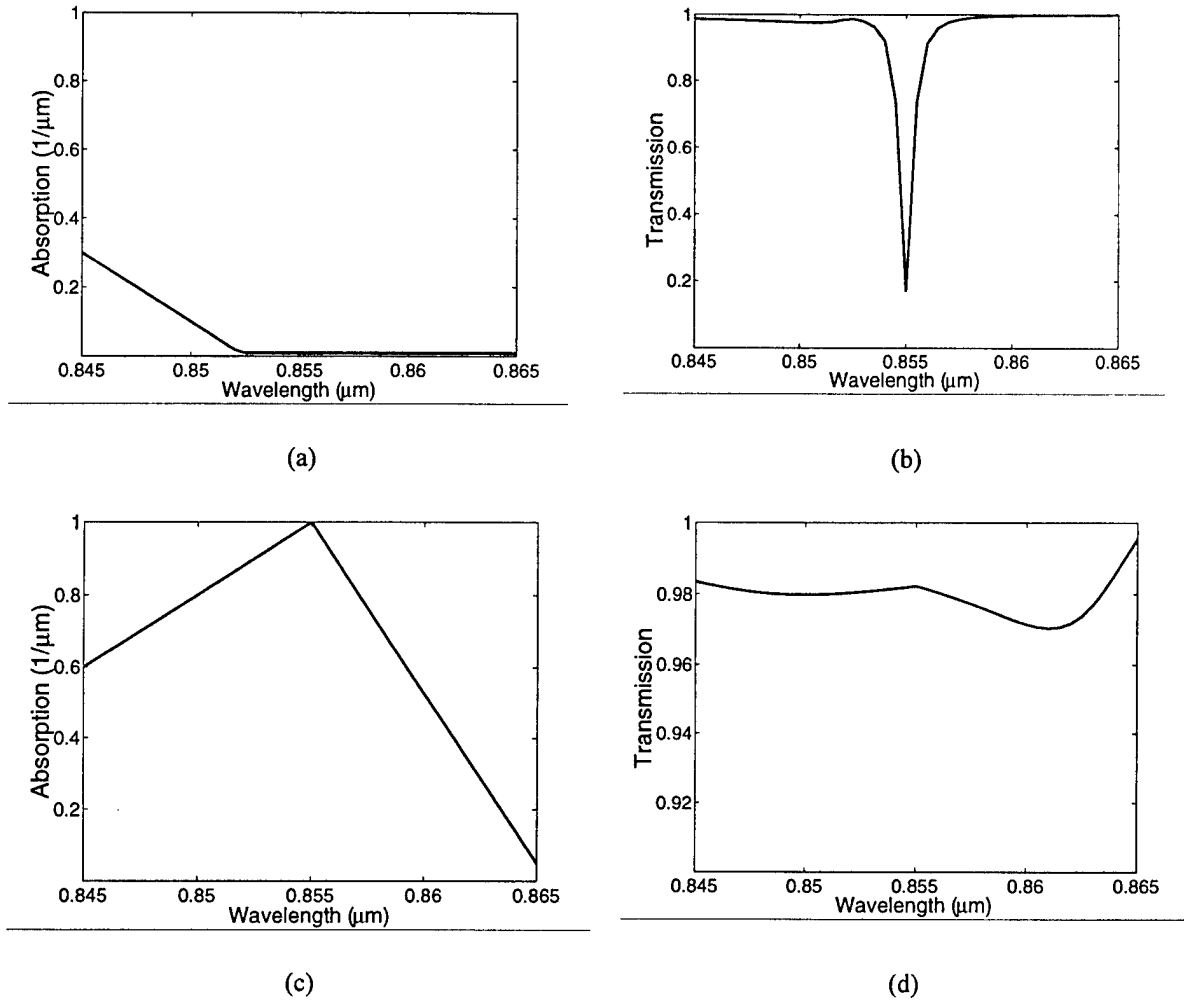
(a)

(b)

(c)

(d)

Fig. 3-6. An illustration of the "double-dip" effect in the experimental transmission spectra: (a) and (c) are the assumed wavelength-dependent ARROW propagation loss at two different biases; (b) and (d) show the corresponding transmission spectra calculated with the coupled-mode equations and the dispersion relations shown in Fig. 3-4. The assumed coupling coefficient is 3mm^{-1}, and the interaction length is 1mm.

With the development of silicon V-groove technology, fiber half couplers with arbitrary interaction lengths and polishing depths can be realized. The increase in the interaction length will lead to devices with much larger on/off ratios. As shown in Fig. 3-7, a 5mm long device with otherwise identical parameters as the one in Fig. 3-6, has a calculated on/off ratio of more than 40dB (10000:1).
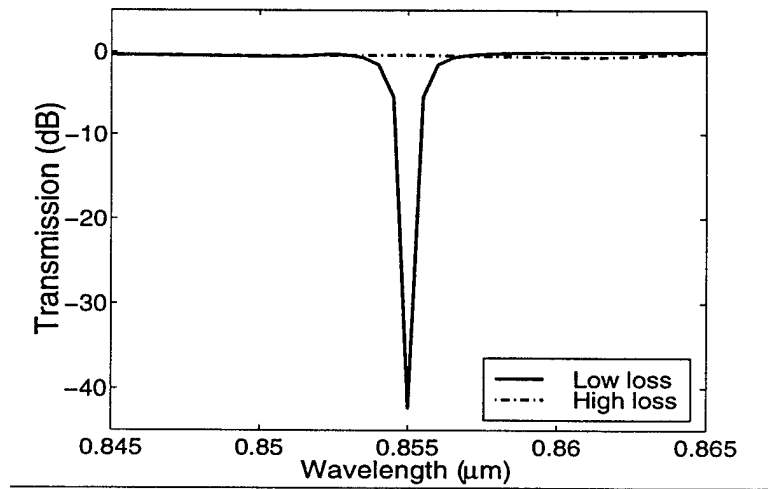
Fig. 3-7. The transmission spectra of a 5mm long in-line modulator, as calculated with the coupled-mode equations. The low- and high-loss cases correspond to the ARROW absorption curves shown in Fig. 3-6a and 3-6c.

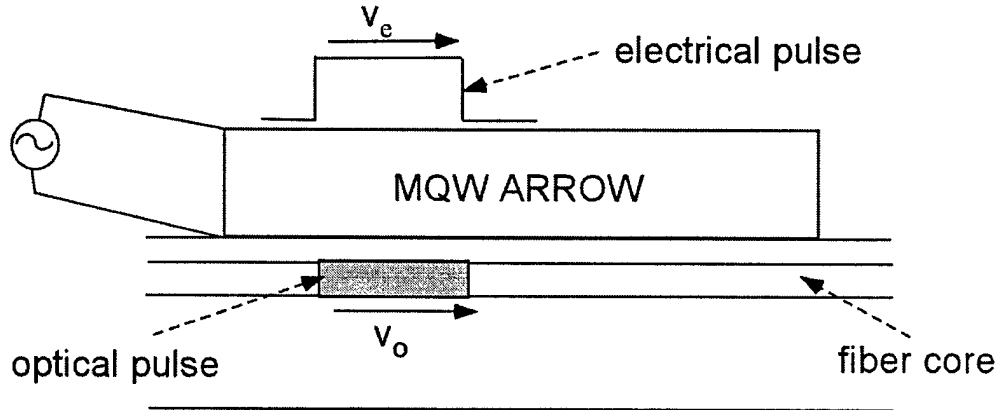## 3.5 Simulation of traveling wave modulators

Fig. 3-8. The concept of a traveling wave modulator: the modulation signal (electrical) travels at the same speed as the modulated signal (optical).

The speed of our lumped-element device is limited by its RC time constant. The capacitance of the device can be estimated as

$$C = \frac{\varepsilon_r \varepsilon_0 A}{d},$$
(3-1)

where ε_r is the relative permittivity of GaAs, ε_0 is the free space permittivity, A is the area of the device and d is the thickness of the intrinsic region. The smallest possible device area is determined by the size of the fiber core and the interaction length. With a 1mm interaction length and a 5μm fiber core diameter, $A = 1mm \leftarrow 5\mu m$, $\varepsilon_r = 13$, and d=0.4μm, the minimum capacitance is about 1.5pF. Ignoring other resistances, and with a microwave source impedance of 50Ω, the RC time constant is 75ps, which means a bandwidth of about 13GHz. The practical limit, however, is expected to be much lower than this, mainly due to parasitics as well as transmission line effects which can be appreciable at these dimensions (with a microwave propagation index of 10, a 13GHz signal has a wavelength of 2mm in the medium). In order to increase the operating speed, a traveling wave electrode design is needed. In this case, when a voltage pulse is applied to the ARROW, it travels along the waveguide, together with the optical signal (Fig. 3-8). When the propagating velocities of the two signals are matched and when the voltage pulse travels without loss, the device will have no bandwidth limitations.
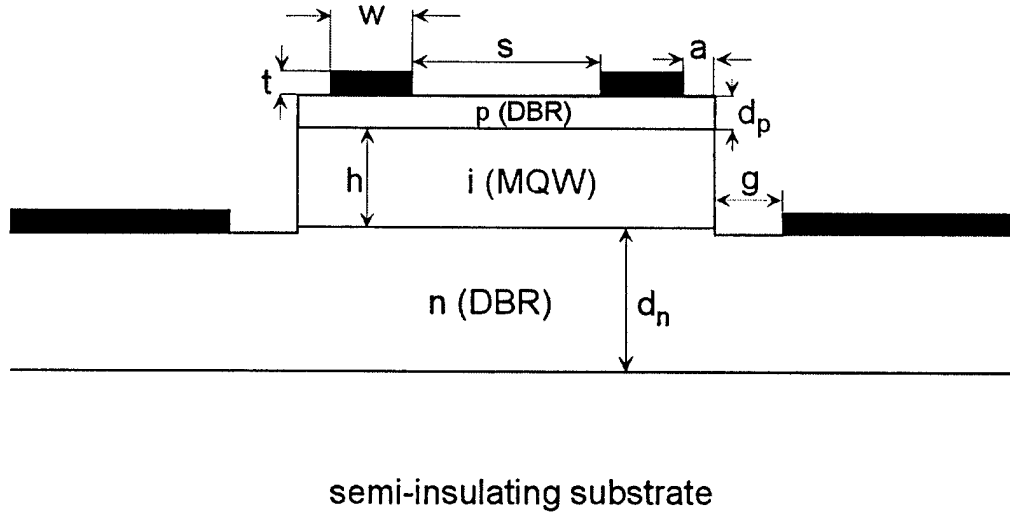
3.5.1. Electrode design

Fig. 3-9. The cross-sectional view of a traveling wave electrode design for an in-line fiber modulator.

A traveling wave electrode design, taking into account such practical considerations as processing constraints and sufficient space for the fiber interface, is shown in Fig. 3-9. The roughly optimized numerical values for the dimensions are: $w = 3\mu m, t = 1\mu m, s = 9\mu m$, $a = 2\mu m$, $h = 1\mu m$, $g = 3\mu m$, $d_p = 0.15\mu m$, and $d_n = 2\mu m$. The contact metal is gold, with a conductivity of $4.4 \times 10^7 S/m$. The doping levels for the n-type and p-type DBRs are $1 \times 10^{18} cm^{-3}$ ($\sigma_n \approx 5 \times 10^4 S/m$) and $1 \times 10^{19} cm^{-3}$ ($\sigma_p \approx 1 \times 10^4 S/m$), respectively. The center conductor is divided into two parts, leaving a slot in the middle for fiber access.
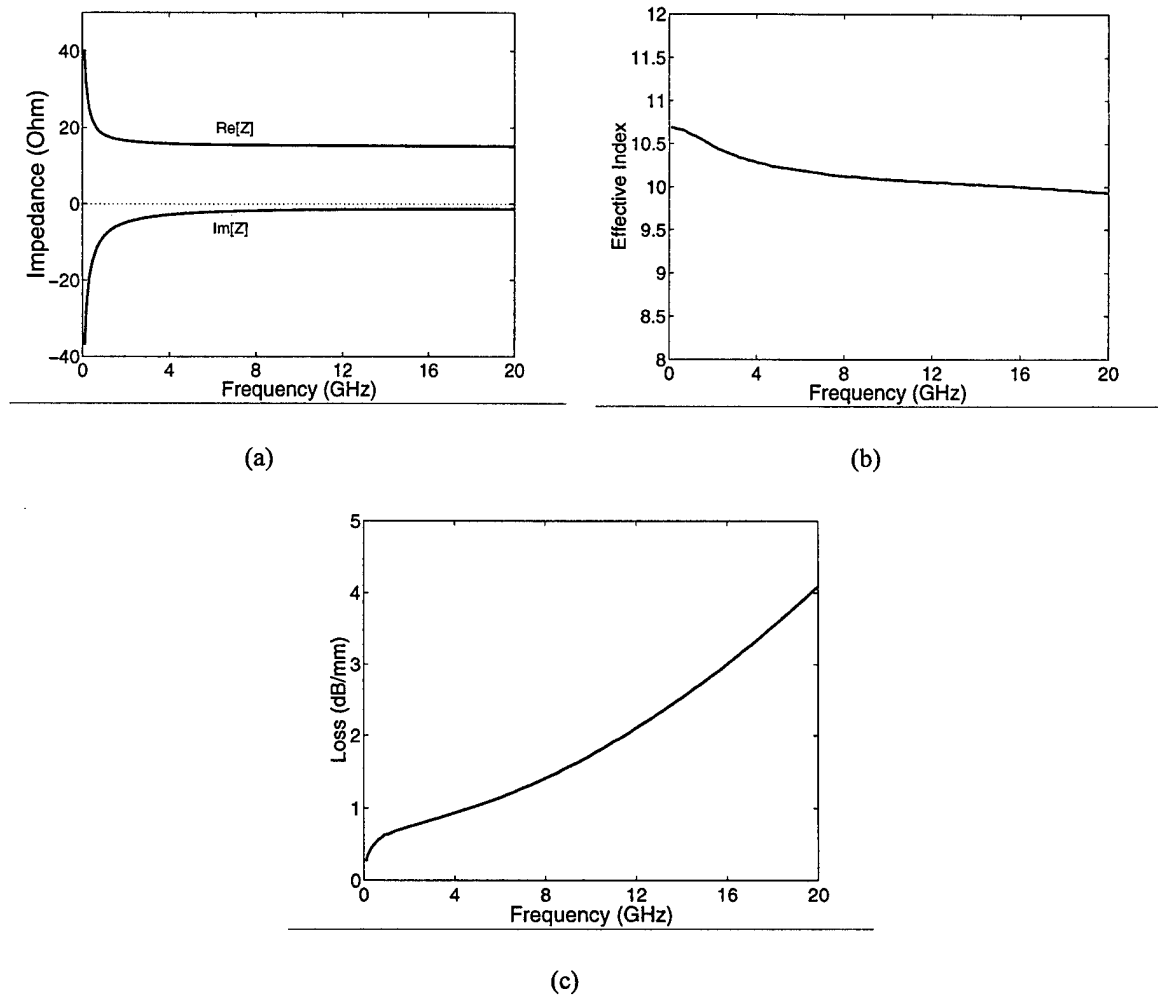

(a)

(b)

(c)

Fig. 3-10. The calculated characteristic impedance (a), effective propagation index (b), and the attenuation coefficient (c) of the traveling wave electrode structure shown in Fig. 3-9.

The propagation characteristics (propagation index, loss and impedance) of the transmission line are calculated using the HP Momentum package within the Hewlett Packard Advanced Design System (HPADS, version 1.1). The software is based on a numerical discretization technique called the method of moments, which is used to solve Maxwell's equations for planar multi-layer dielectric structures. The output of the program is in terms of the S-parameters of the transmission line, which can then be converted into propagation parameters. In Fig. 3-10, the calculated values for the attenuation coefficient, the characteristic impedance and the effective index are plotted as functions of frequency.
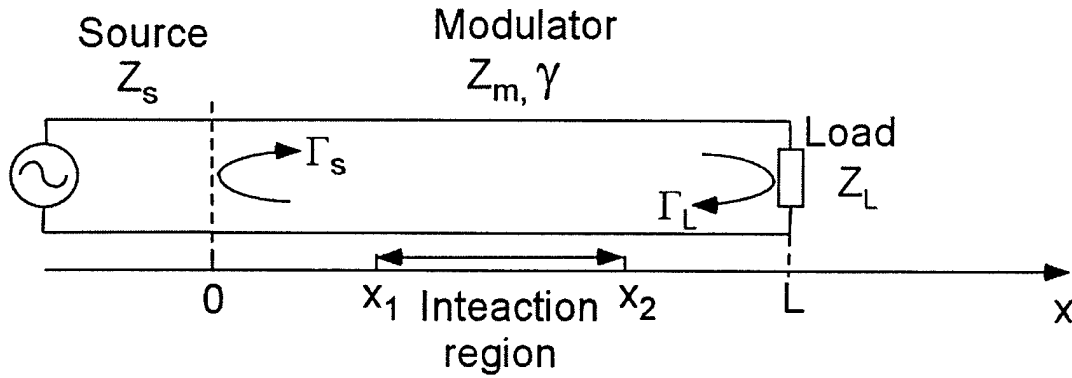
3.5.2 Frequency Response

Fig. 3-11. The transmission line model used to calculate the modulator frequency response.

Assuming that the modulator is linear, then its optical response, R, will be proportional to the "accumulation" of the modulation voltage V_m along the device,

$$R \propto Max \left| \int_{x_1}^{x_2} V_m(x,\phi)dx \right|?, \qquad (3\text{-}2)$$

where x_1 and x_2 are the boundaries of the interaction region, ϕ is a phase variable. By varying the value of ϕ from 0 to 2π, a maximum value of the integral can be obtained, which corresponds to the device response. Using the model shown in Fig. 3-11, and taking into account multiple microwave reflections inside the modulator, V_m can be expressed as

$$V_m(x,t,\phi) = \text{Re}\, \frac{V_0 T\{\exp(-\gamma x) + \Gamma_L \exp(\gamma x - 2\gamma L)\}\exp(j\omega t + \phi)\}}{1 - \Gamma_s \Gamma_m \exp(-2\gamma L)} , \qquad (3\text{-}3)$$

where V_0 is microwave source voltage, T is the transmission coefficient from the source to the modulator, Γ_s and Γ_L are the reflection coefficients at the source and the load, respectively, γ is the complex microwave propagation coefficient, and ω is the microwave frequency. In terms of the impedances, the expressions for the T, Γ_s and Γ_L are

$$T = \frac{2Z_m}{Z_m + Z_s} , \qquad (3\text{-}4)$$

$$\Gamma_s = \frac{Z_s - Z_m}{Z_s - Z_m} , \qquad (3\text{-}5)$$

$$\Gamma_L = \frac{Z_L - Z_m}{Z_L - Z_m} . \qquad (3\text{-}6)$$

The complex propagation coefficient γ is given by,

$$\gamma = \alpha_\mu + j\frac{\omega}{v_\mu} , \qquad (3\text{-}7)$$

where α_μ is the microwave attenuation and v_μ is the microwave phase velocity.

When an optical pulse starts to propagate with optical group velocity v_0 at $t=0$ and $x=0$, it reaches position x at $t = x/v_0$, at which point the modulation voltage it sees is $V_m(x,\phi) = V_m(x,t = x/v_0,\phi)$. Therefore the modulator response can be expressed as

$$R \propto Max \left| \int_{x_1}^{x_2} V_m(x,t = x/v_0,\phi)dx \right|? . \qquad (3\text{-}8)$$

In an ideal traveling wave modulator, $\alpha_\mu = 0$, $v_0 = v_\mu$, $\Gamma_s = \Gamma_L = 0$, and $T=1$, so $V_m(x,t,\phi) = V_0\cos\phi$ and $R \propto |V_0(x_2 - x_1)|$ (obviously the integral reaches its maximum value when $\phi = 0$). As the situation deviates from the ideal case, the modulation voltage seen by the optical pulse becomes position dependant and the response decays.
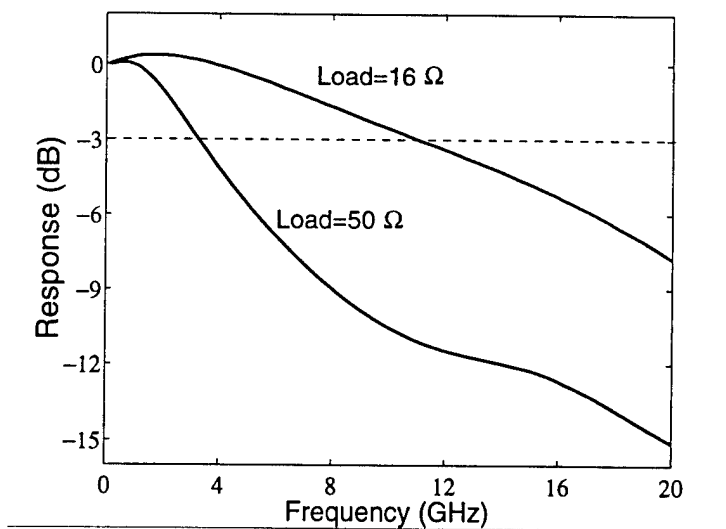
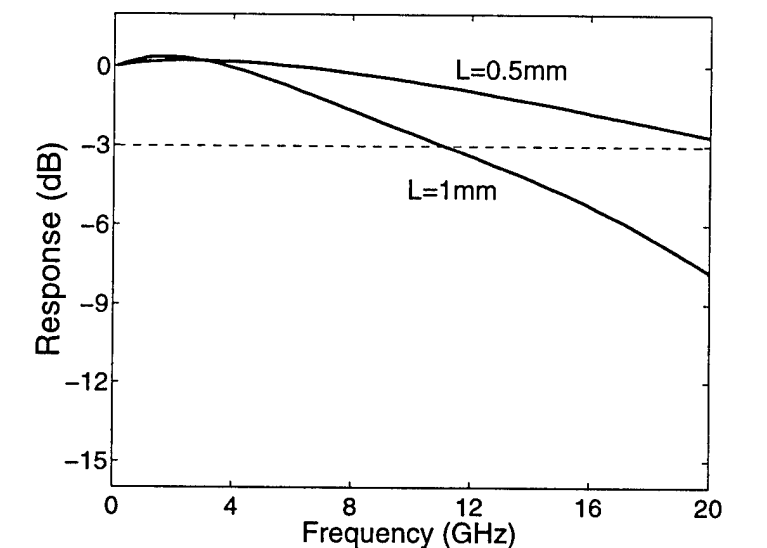Fig. 3-12. The calculated frequency responses for a 1mm long modulator.

Fig. 3-13. The calculated frequency responses for devices with different interaction lengths.

In Fig. 3-12, the calculated frequency responses for a 1mm long device are plotted. When the load impedance (50Ω) is different from the characteristic impedance of the transmission line (~16Ω), a standing wave pattern is created along the interaction region, which degrades the frequency response and lowers the device bandwidth. Fig. 3-13 shows that a 0.5mm device has a 3dB bandwidth of greater than 20GHz compared with

11GHz for a 1mm device. The drawback, though, is that a shorter device will have a lower modulation contrast.

Chapter 4 In-line fiber light emitter

4.1 Introduction

All devices described so far operate via the coupling of light from the fiber into the ARROW. A coupled waveguide system, upon whose physics all these devices are based, however, is by no means a "one-way street" (i.e., light can travel the other way too). In fact, if the ARROW can be made to generate light or provide optical gain, the ARROW-fiber coupled waveguide structure could become a new device paradigm for fiber-coupled narrowband optical communication sources or in-line fiber optical amplifiers. In this chapter, a proof-of-concept in-line fiber light emitter is presented.

4.2 Device design and experiment

The epitaxial structure used for this experiment is the same as that of the detector (Fig. 2-6). By forward biasing the p-i-n diode, electrons and holes are injected into the intrinsic region and most of them recombine in the quantum well, creating photons. The photons are emitted into multiple modes, and only those that are phase-matched to the fiber mode are coupled into the fiber. Therefore, a narrowband output from the fiber is expected.

After the wafer was grown, proton implantation, which converts doped layers into highly resistive layers by creating defects that trap electrons and holes, was performed as the first processing step to provide electrical isolation and current confinement. As a result of these implantation steps, the p-type mirror was rendered electrically insulating and current injection only occurs at regions in the vicinity of the fiber core (Fig. 4-1), thus the efficiency of the device can be improved. The processing and testing steps that followed were the same as those used for the detector, with the exception that the ARROW was forward biased. The optical output in the fiber was observed with an optical spectrum analyzer.
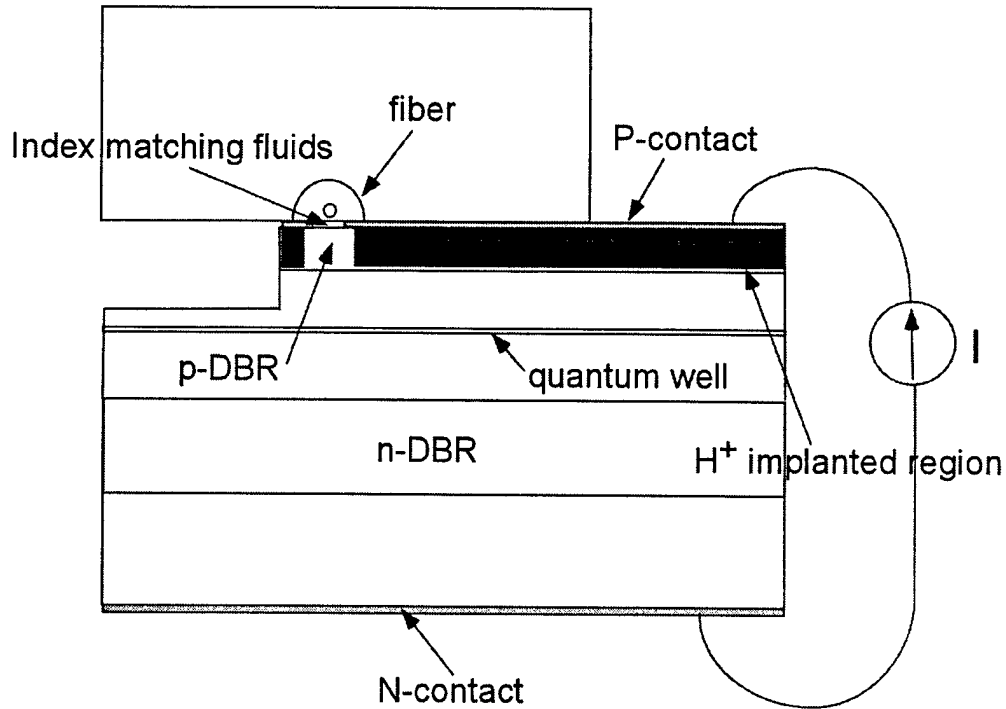
25

Fig. 4-1. The cross-sectional view of the light-emitting device testing arrangement.

6.2 Results and discussion

The observed output spectra as a function of injection currents is shown in Fig. 4-2. The two groups of emission peaks correspond to TE and TM resonances. The TE resonances have narrower linewidths mainly because of the higher reflectivity of the DBR mirrors, and hence lower ARROW propagation losses. The total output power measured with an optical power meter was about 7nW for an injection current of 100mA. This amount of current results in the injection of about 10^{18} electron-hole pairs per second, which ideally would create an equal number of photons per second. At the photon energy of 1.5eV (~830nm), 10^{18} photons per second corresponds to a power of about 200mW. Therefore, discounting any non-radiative recombination, the emission efficiency, which is defined as the ratio of the number of photons detected in the fiber to the number of photons generated in the ARROW, could be as low as 3×10^{-8}.
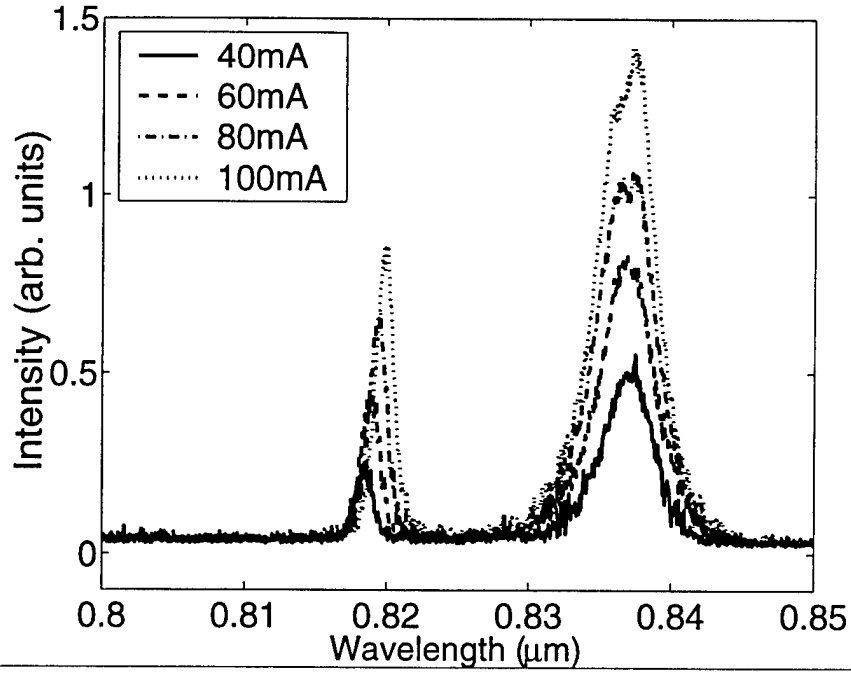
Fig. 4-2. The measured emission spectra as a function of injection currents.

This low efficiency is not surprising since there is no lateral optical confinement defined in the ARROW. Therefore photons can be emitted at angles that are not collinear with the fiber. By lithographically defining a lateral waveguide, the two-dimensional photonic density of states can be reduced to a one-dimensional one, and the number of modes into which photons can be spontaneously emitted is further restricted. However, as with other microcavity devices, there is always the challenge of reducing dimensions without increasing surface trap states which can lead to non-radiative recombination.

The measured transmission spectra under different current injection levels are shown in Fig. 4-3. Due to heating problems, our devices could not sustain more than 100mA. Under this injection level, no transmission gain was observed because there were not enough injected carriers to overcome the quantum well absorption loss. The sheet carrier density in the quantum well can be estimated as follows:

$$n = \frac{J\tau}{e}, \qquad (4-1)$$

where J is the injection current density, τ is the carrier lifetime and e is the electronic charge. The non-implanted area of the ARROW was 2mm by 50μm, therefore 100mA of

27

current corresponds to a current density of $100A/cm^2$. Assuming all carriers recombine in the quantum well with a lifetime of 0.5ns, the sheet carrier density is about $3\times10^{11}cm^{-2}$, which is about an order of magnitude less than the injection level needed for transparency (i.e., loss=0).

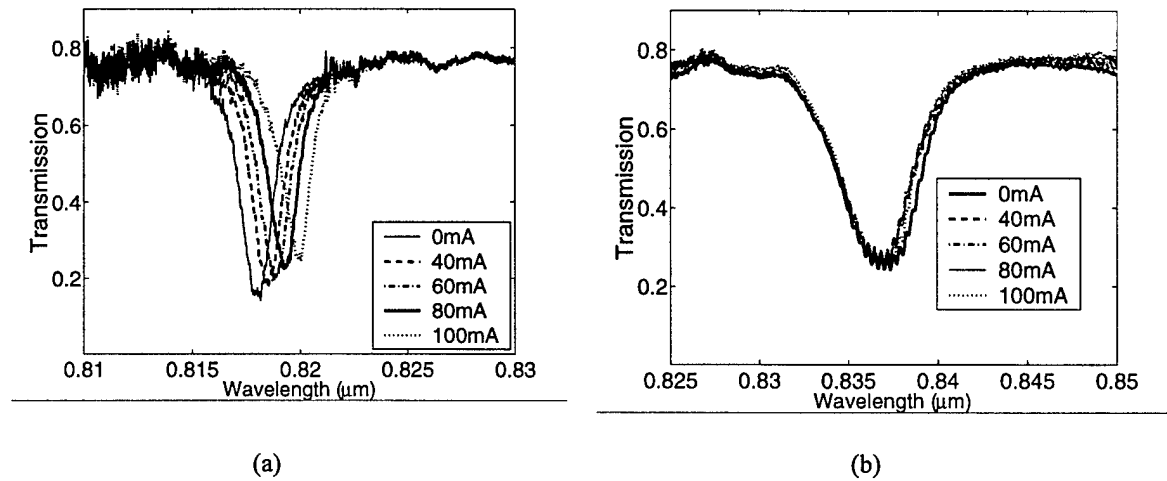(a)   (b)

Fig. 4-3. The transmission spectra under different current injection levels for TE polarized light (a) and TM polarized light (b).
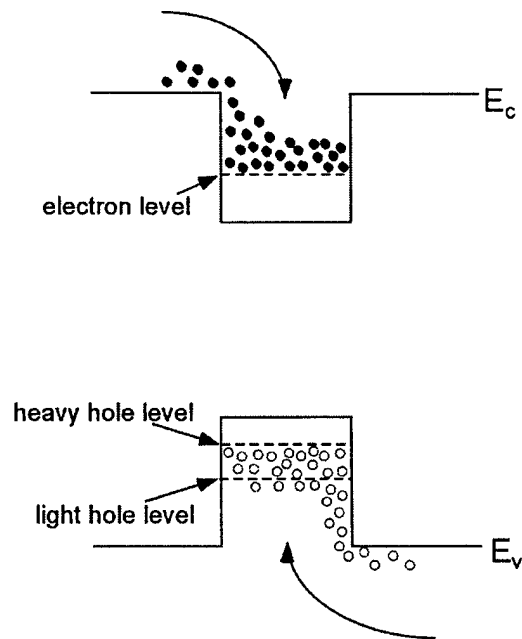

Fig. 4-4. The band diagram of a semiconductor quantum well. The split in the heavy and light hole bands results in most injected holes falling into heavy hole states.

28

The shift in the TE spectra is due to carrier induced refractive index change in the quantum well. There is hardly any change in the TM spectra, however, and that can be attributed to the split in the heavy and light hole bands in the quantum well. At the present injection level, most holes injected into the quantum well occupy heavy hole states because of their lower energies (Fig. 4-4). For TM polarized light, only the light hole transitions are allowed. Therefore changes in the injection current result in much larger absorption (and index) changes for TE polarized light than for TM polarized light. This effect is also confirmed by the luminescence data (Fig. 4-2) where the TE emission peak red-shifts with increasing current, while the TM peak does not move.

Chapter 5 Conclusion

We have demonstrated proof-of-concept in-line fiber devices based on evanescent wave coupling between single mode fibers and semiconductor (GaAs) waveguides. This type of device promises to alleviate the problems of high insertion loss and high cost associated with conventional fiber device packaging, as well as to create a new device paradigm for wavelength division multiplexing applications. Due to the large index difference between glass and GaAs, DBR mirrors have to be used in the GaAs waveguide so that phase-matching can be achieved. The mirrors are designed to provide high reflection for a specific mode angle, therefore the optical wave inside the GaAs waveguide can propagate with an effective index that is much lower than the material index.

The experimental demonstration of a narrow linewidth filter (FWHM=0.5nm near 830nm for TE light) verified the properties of the in-line device structure. By including a quantum well absorbing layer in the core of the ARROW, a wavelength selective photodetector (FWHM=1.6nm) was demonstrated.

Next, an in-line fiber intensity modulator utilizing the quantum confined Stark effect was investigated. A multiple-quantum-well layer, whose absorption coefficient and refractive index can be changed under the influence of a vertical electric field, was placed in the ARROW core. The electric field changes the fiber transmission spectrum, therefore intensity modulation at a given wavelength is obtained. The demonstrated device had a maximum on/off ratio of 4:1 with an applied voltage of 9V. Calculations showed that traveling wave electrodes on the ARROW are needed to obtain a high device switching speed. The speed is primarily limited by the microwave propagation loss and the speed mismatch between the microwave and optical signals. The calculated 3dB cut-off bandwidth for a 1mm long device is 11GHz.

Finally, a resonant light emitter was demonstrated by injecting current into the ARROW (same structure as the detector). Emitted photons at phase-matched wavelengths were coupled into the fiber. The current injection also resulted in transmission modulation due to carrier induced index shift.